Fermi National Accelerator Laboratory

Photon Production at CDF and DØ

Presented by Robert M. Harris
For the CDF and DØ Collaborations

*Fermi National Accelerator Laboratory
P.O. Box 500, Batavia, Illinois 60510*

April 1994

Disclaimer

Photon Production at CDF and D0

Presented by Robert M. Harris
Fermi National Accelerator Laboratory
Batavia, Illinois 60510

For the CDF and D0 Collaborations

ABSTRACT

We present measurements of isolated prompt photon production in $\bar{p}p$ collisions at $\sqrt{s} = 1.8$ TeV from the Fermilab experiments CDF and D0. Precision measurements of prompt photon production from CDF constrain the gluon distribution of the proton, and recent results from D0 agree with CDF and QCD. The pseudorapidity distribution of the jet in photon events at CDF is used to constrain parton distributions. Gauge boson $(g,\gamma,W) + $ jet angular distributions at CDF show good agreement with QCD and illustrate the spin of quarks and gluons. Diphoton candidate mass distributions from CDF are used to search for new physics and measure the background to Higgs$\rightarrow \gamma\gamma$. Finally, CDF searches for resonances in the W+jet and γ+jet mass distributions, and thereby excludes excited states of composite quarks for mass $M^* < 540$ GeV/c^2 at 95% confidence level.

1. Isolated Inclusive Photon Production

1.1. Motivation and Theory

Prompt photon production at the Fermilab Collider is a precision test of QCD. Because of the dominant compton diagram, shown in Fig. 1a, prompt photons probe the gluon distribution of the proton at low x ($.01 < x_T < .1$). Some typical diagrams from a next-to-leading-order (NLO) QCD calculation [1] are shown in Fig. 1.
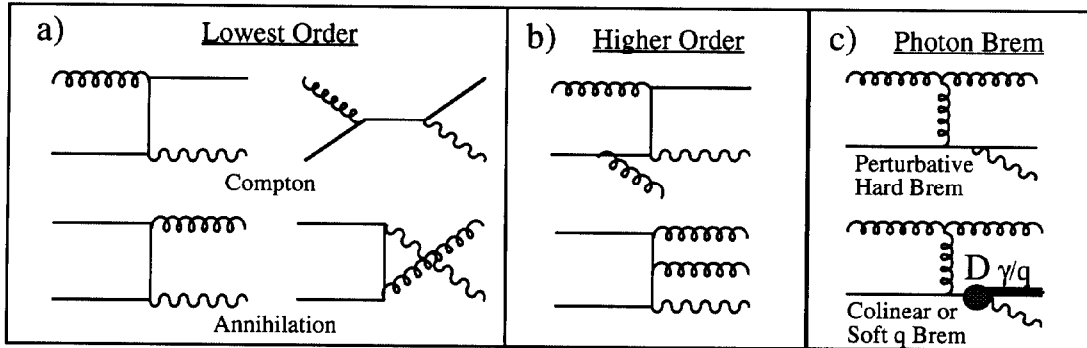

Figure 1: γ production: **a)** Lowest order diagrams. **b)** Some higher order diagrams **c)** Some bremsstrahlung diagrams: one strictly perturbative and one with a photon fragmentation function.

1.2. Data Sample and Event Selection

To measure prompt photons both CDF [2] and D0 [3] employ EM calorimeters segmented into towers in $\eta\phi$ space. The background from neutral mesons π^0, η and K^0_S in jets was supressed by requiring the photon candidate to be isolated: CDF required less than 2 GeV in a cone of radius 0.7 in $\eta\phi$, D0 required less than 2 GeV in the annulus between $R = 0.2$ and $R = 0.4$. Both experiments (CDF, D0) required the photon candidate to have little hadronic energy (HAD/Total<11%, 4%), be neutral (no track, dE/dX separation), have good shower profile (strip χ^2, depth+transverse χ^2), rejected cosmic ray muon bremsstrahlung ($\not{E}_T/E_{T\gamma} < 0.8$, 0.5), required central photons ($|\eta| < 0.9$, 0.9), and had three trigger thresholds in P_T. CDF also required no extra local energy depositions in the CES(see fig. 2) greater than 1 GeV, an event z vertex within 50 cm of the center of the detector, and CDF had an isolation cut in its hardware trigger which allowed it to acquire more photon data at low Pt. For this analysis CDF used 0.06 pb^{-1} above 6 GeV, 18 pb^{-1} above 16 GeV, 21 pb^{-1} above 50 GeV and D0 used 0.005 pb^{-1} above 6 GeV, 0.022 pb^{-1} above 14 GeV, and 3.86 pb^{-1} above 30 GeV.
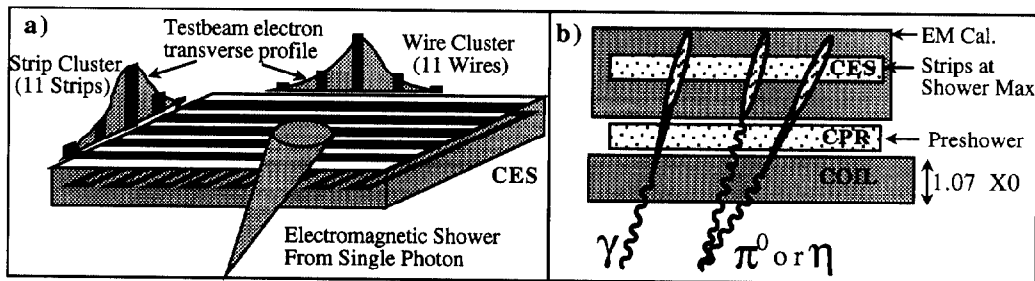

Figure 2: CDF background subtraction: **a)** The profile method and **b)** the conversion method.

1.3. CDF Background Subtraction

After all cuts a background predominantly from isolated π^0 and η mesons remains. To remove this background CDF employs two methods, the profile method uses the transverse profile at shower maximum (in the CES) and the conversion method uses photon conversions occurring in the solenoidal coil and measured in a preshower detector (the CPR). Fig. 2a illustrates the profile method in which we fit the transverse profile to a testbeam shower and obtain a χ^2 which is larger for π^0 and η mesons than for single photons. Fig. 2b illustrates the conversion method in which the probability of measuring a conversion in the CPR is higher for a π^0 or η meson than for a single photon. In Fig. 3 we show the efficiencies of the methods for photon candidates (the data) and for simulated photons and background. The fraction of photons in the data is $f = (\epsilon - \epsilon_B)/(\epsilon_\gamma - \epsilon_B)$, where ϵ, ϵ_γ and ϵ_B are the method efficiencies for photon candidates, pure photons, and pure background respectively.
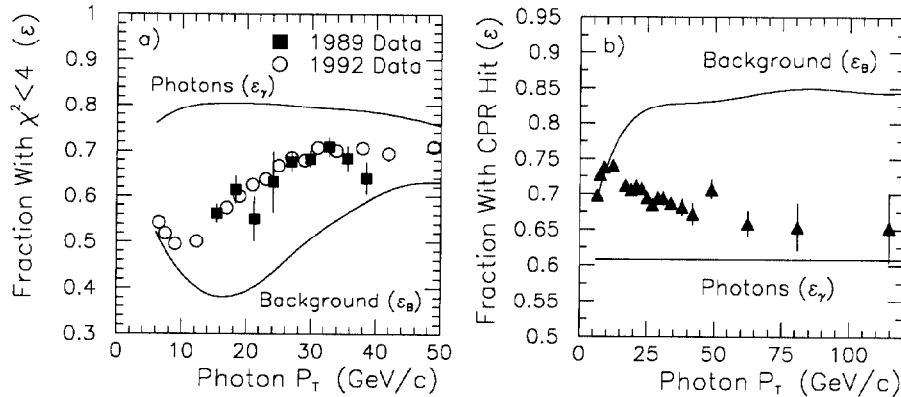

Figure 3: CDF background subtraction efficiency ϵ for photon candidates (points) compared with simulated photons and background for a) the profile method and b) the conversion method.

1.4. CDF Inclusive Photon Results

In Fig. 4a we show the cross section from the two methods separately; in the overlap region they agree to within 5%. Although there is qualitative agreement between data and the
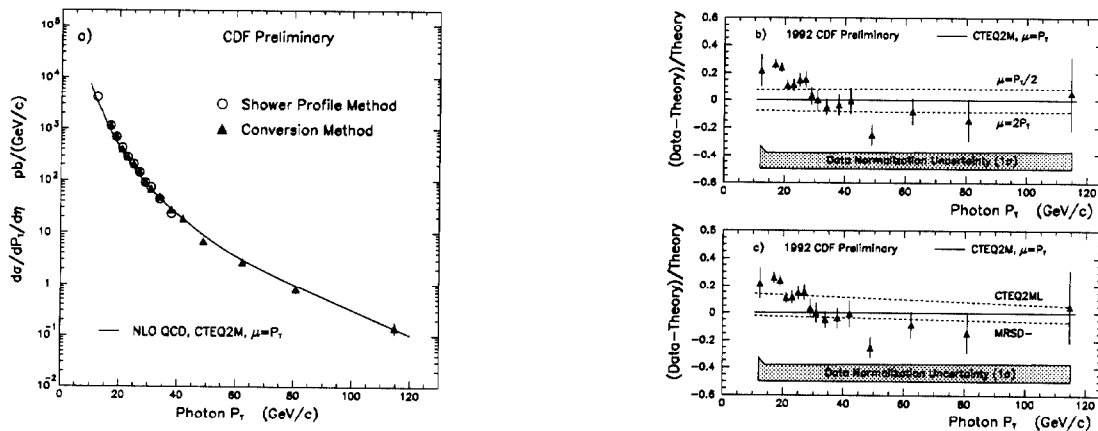

Figure 4: The isolated photon cross section from CDF a) showing both methods of background subtraction and b) the fractional difference with QCD using difference choices of renormalization scale and c) parton distributions.

QCD prediction [1] on a logarithmic scale, in Fig. 4b,c we show that the data has a steeper slope

at low P_T regardless of the choice of parton distribution or renormalization scale. This result is similar to that previously reported, [4] and may indicate a more singular gluon distribution than given by existing parton distribution sets.

1.5. CDF Calibration and Uncertainties

The uncertainties shown in Fig. 4b,c by the shaded band are completely correlated as a function of P_T. The small level of uncertainty results from studies on large samples of fully reconstructed π^0, η and ρ mesons shown in Fig. 5a,b. These samples provide three independent calibrations of the conversion rate measured in the preshower, presented in Fig 5c, which all agree with expectations from the amount of material and the details of the meson decay. This
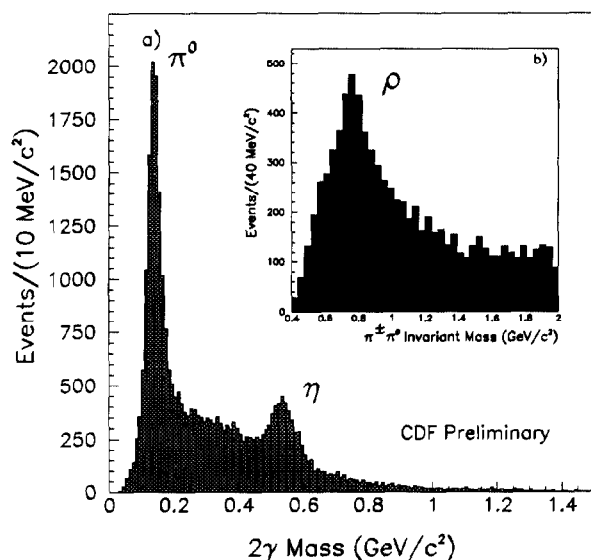
c)   Calibration and Uncertainties

CDF Conversion Rates from Preshower

	Measured	Expected	Difference
π^0	.842±.008	.847±.006	−.005±.010
η	.831±.012	.842±.006	−.011±.013
ρ	.836±.010	.834±.006	+.002±.012

CDF Systematic Uncertainties
in Cross Section from Conversion Method

Source	Pt=16 GeV	Pt=100 GeV
Conversion Rate	7%	4.5%
Backscattering	2%	7%
Luminosity	6.8%	6.8%
Cut Efficiencies	4.8%	4.8%
Energy Scale	4.5%	4.5%
Total	12%	13%

Uncertainties at Colliders (P$_T$ =16 GeV)

	Statitstical	Systematic
CDF (Preliminary)	2.6%	12%
UA2	6%	21%
UA1	9%	29%
D0 (Preliminary)	12%	53%

Figure 5: a) Two photon mass data showing π^0 and η mesons. b)Track + π^0 mass data showing charged ρ mesons. c) Comparison of conversion rates from the meson samples with expectations, resulting systematic uncertainties, and CDF uncertainties compared with other experiments.

results in small systematic uncertainties. Fig 5c compares photon uncertainties among collider experiments, and shows that CDF has made a precision measurement of photon production.

2. D0 Photon Measurement

In Fig. 6a we outline the D0 background subtraction method which measures conversions in the central drift chamber. The conversions occur in the material of the vertex drift chamber and transition radiation detector. Since D0 is measuring tracks they use dE/dX to separate electrons from photons. In the future D0 will measure conversions in their 1st EM depth segment, where the increased material will allow a better γ-π^0 separation. One important difference between CDF and D0 measurements is that CDF measures the γ fraction for each P_T bin independently, while D0 fits their γ fraction vs. P_T and uses the fit to determine the cross section. This effectively smooths the D0 statistical errors down by roughly a factor of five, moving the statistical error on the background into a systematic error on the photon cross section. The resulting D0 cross section, shown in Fig. 6b, is in good agreement with both the CDF result and the NLO QCD prediction.

a) D0 Background Subtraction

• <u>Now: Conversions measured in Central Drift Chamber</u>

EM Calorimeter

Cen. Drift Chamber — EM1 (2 X0)

Trans. Rad. Det. — ~ 0.1 X0

Vertex Drift Chamber

γ π^0 or η e
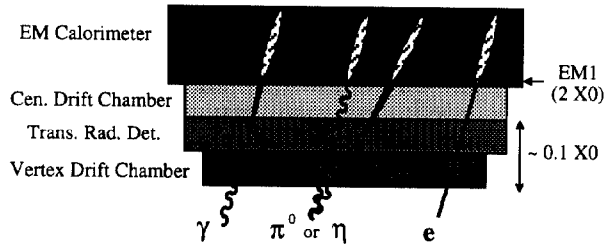
♦ Conversions in material of VTX + TRD to separate
  γ (P=12+/-1%) from π^0 (P≈23%).

♦ dE/dX in CDC to separate e (~1 mip) from γ (~ 2 mips).

• Soon: D0 will use conversions measured in 1st EM Depth Segment.

♦ 2X0 gives Pγ ~ 0.8 and Pπ^0 ~ 0.95
    ⇒ better separation with lower statistical errors.

b)

▲ CDF PRELIMINARY
  12% Normalization Uncertainty

⊙ D0 PRELIMINARY
  Inner Errors — Statistical
  Outer Errors — Systematic

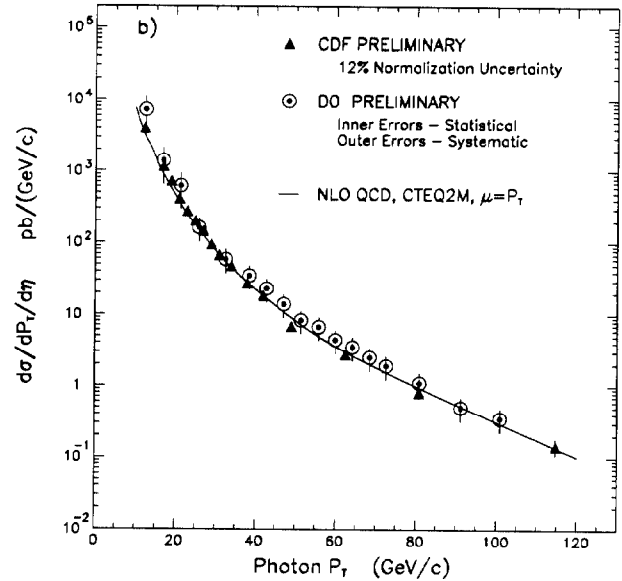— NLO QCD, CTEQ2M, μ=P$_T$

Photon P$_T$ (GeV/c)

Figure 6: a) D0 background subtraction and b) cross section compared to CDF and QCD.

3. Photon + Jet Pseudorapidity

Measuring the pseudorapidity of the recoiling jet, η_J, in photon events gives more information on parton x. Forward jets probe both lower and higher values of x than central jets. CDF uses the conversion method analysis for photons in the range $16 < P_{T\gamma} < 40$ GeV/c and requires the jet be back to back with the photon, $150° < \Delta\phi_{\gamma J} < 210°$. The $\Delta\phi_{\gamma J}$ cut minimizes corrections to the η_J distribution which are made for the effects of η_J resolution smearing and leading jet misidentification near cracks. These corrections are necessary because of poor jet energy resolution coupled with the presence of extra jets from the underlying event and $\gamma + 2$ jet events. The pseudorapidity distribution of the highest E_T jet in photon events is shown in Fig. 7a, and compares well with NLO QCD. In Fig. 7b we show the ratio of data to QCD and also present our systematic uncertainties from the η_J resolution unsmearing procedure. The data has sufficient precision to separate among different parton distribution sets and currently favors CTEQ2M [5] and MRSD0. [6]
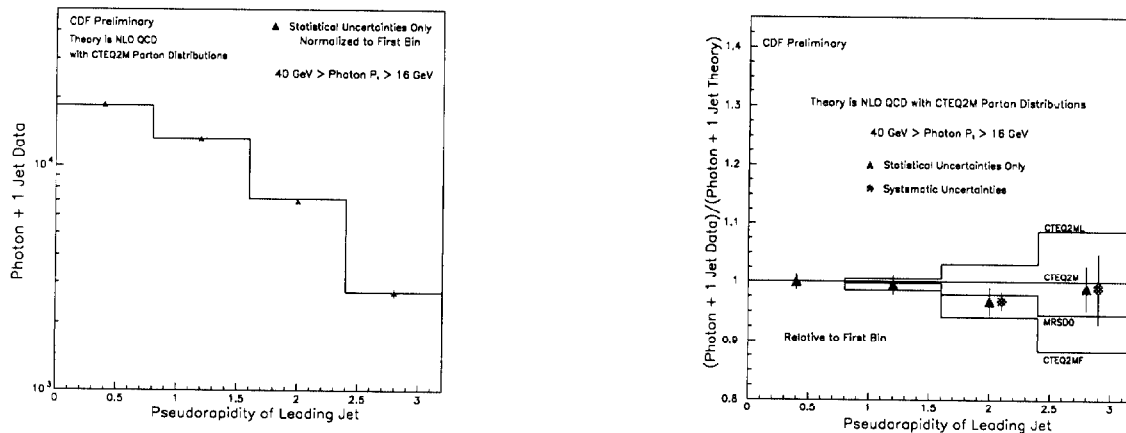

Figure 7: a) The jet pseudorapidity in CDF photon events (points) compared to NLO QCD (histogram). b) The ratio of data to NLO QCD (CTEQ2M) and the ratio of various parton distribution sets to CTEQ2M. Statistical and systematic uncertainties are shown separately.

4. Gauge Boson + Jet Angular Distribution

CDF has published dijet and photon + jet angular distributions and we have recently analyzed the W + jet angular distribution. As sketched in Fig. 8a, we boost from the lab to the center of momentum frame, and θ^* is the angle between the gauge boson (γ, g, W) and the beam line. In the W + jet analysis, we mass constrain the electron and neutrino to the W mass, and this gives two solutions for the z component of the neutrino momentum, and hence also for $\cos\theta^*$. We choose the solution with $\cos\alpha > 0$, where α is shown in Fig. 8a. The dijet, photon+jet and W+jet angular distributions are shown in Fig. 8b compared to QCD predictions. The dijet angular distribution is essentially Rutherford scattering, and peaks sharply near $|\cos\theta^*| = 1$, while γ+jet and W+jet angular distributions are flatter. This is caused by the different spins of quark and gluon propagators, as shown in the Feynman diagrams at the bottom of Fig. 8a.
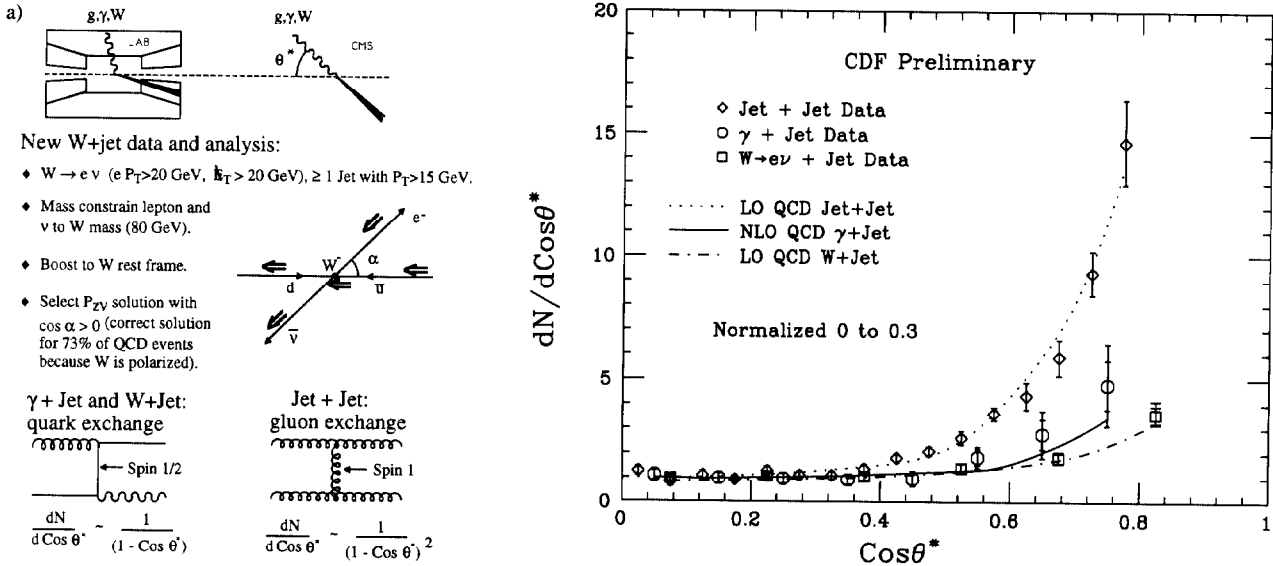

Figure 8: a) Gauge boson + jet angular distribution analysis (concentrating on W+jet). b) CDF angular distributions for dijet, [7] γ + jet, [8] and W + jet events is compared to QCD predictions.

5. Diphotons

Measurements of diphotons test NLO QCD [9] processes which are a background to Higgs$\rightarrow \gamma\gamma$. Diphotons can also be used to search for exotic objects. Among the three processes shown in Fig. 9a, the Born diagram dominates at high mass. Unlike the previously published CDF diphoton analysis, [10] this analysis employs a tighter isolation cut (2 GeV in a cone of radius 0.7), includes the background from $\gamma\pi^0$ and $\pi^0\pi^0$ (comparisons are made to QCD + background estimate), and measures data in a higher mass range. This enables us to both test QCD and to search for signals at high mass, where small numbers of events prevent a statistical background subtraction. Analysis of lower mass data with a background subtraction is in progress. The differential mass distribution is shown in Fig. 9b and compares well with the NLO QCD + background estimate except for the last bin. The last two events are best compared to the theory with an integral plot, Fig. 9c, in which it is seen that two events is over an order of magnitude more than predicted. Data from the 1994-95 run, already in progress, should tell us whether the two events at high mass are merely a fluctuation or a sign of new physics. The apparent difference in shape between QCD and data at lower mass on the integral plot results from the affect of the two unexpected events at high mass: the differential plot is more appropriate for a QCD test.
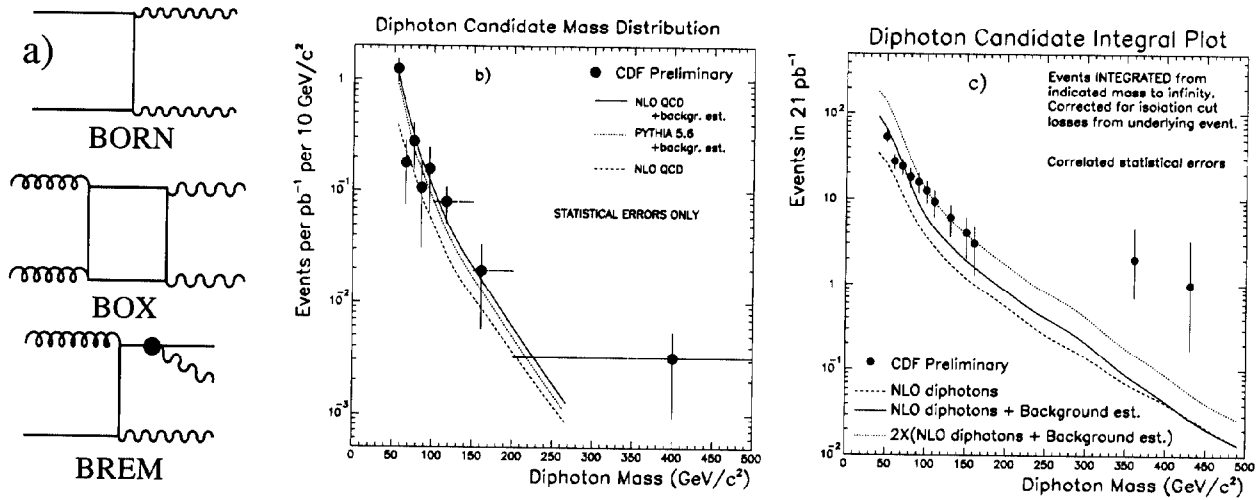
Figure 9: a) Dominant diphoton production diagrams. b) CDF diphoton + background mass distribution compared to QCD + background estimates. c) Integral plot of events from mass M to ∞ (CAUTION: correlated statistical errors).

6. Excited Quark Search

If quarks are composite particles then excited states q^* are expected. [11] Recently, CDF has searched [12] for the mass resonances $qg \rightarrow q^* \rightarrow q\gamma$ and qW. For the photon + jet mass distribution we improved our mass resolution and reduced the systematics by assuming P_T balance between the photon and the leading jet; thus the jet energy was not used to form the photon + jet mass. For the W + jet mass distribution, similar to section 4, we constrain the lepton + neutrino to the mass of the W but here we pick the smaller of the two solutions for the W + jet mass; this reduces mass smearing and fluctuations. For the γ (W) analysis we reduced the QCD background by requiring $|\cos\theta^*| < 2/3(0.9)$. The photon candidate plus leading jet mass distribution and the smaller solution for the W + leading jet mass distribution is shown in Fig. 10 and compare well with QCD predictions leaving little room for a q^* signal. Fitting
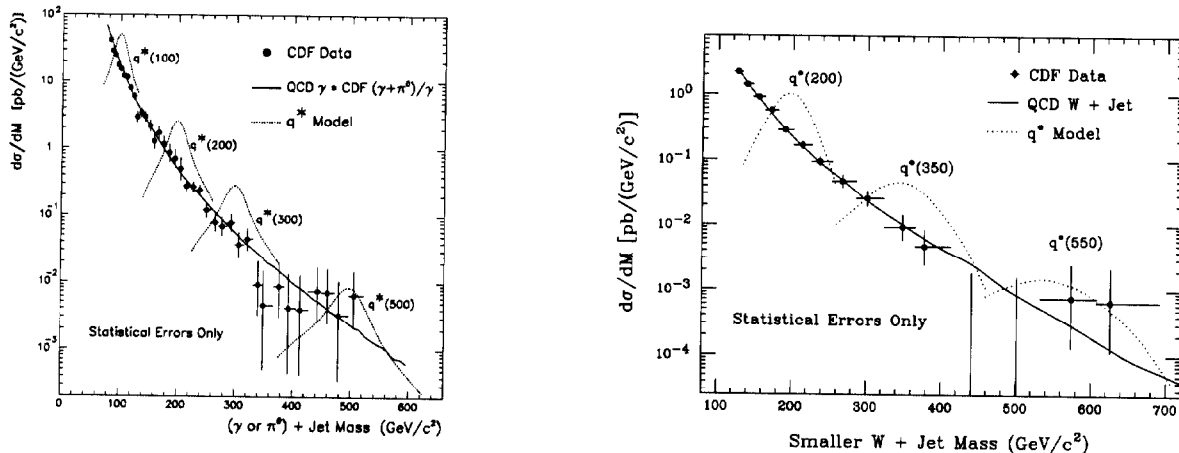

Figure 10: a) Photon candidate + jet mass spectrum and b) W + jet mass spectrum, both compared to QCD background estimates and an excited quark model. [11]

the data to a QCD background + q^* signal hypothesis we find 95% confidence level upper limits on the signal cross section shown in Fig. 11a, which when compared to the q^* model expectation [11] allow us to exclude excited quarks in the mass interval $80 < M^* < 540$ GeV/c^2. The coupling can however be smaller than expected, so in Fig. 11b we show the excluded regions
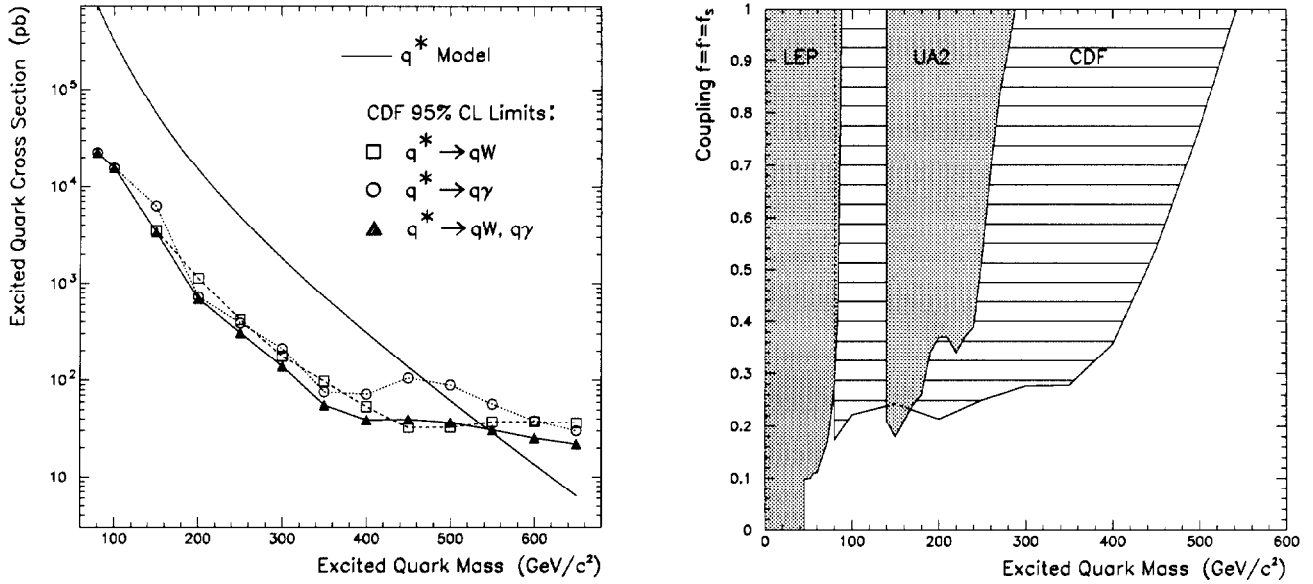
Figure 11: **a)** Cross section limits on excited quark production in the photon, W and combined channels. **b)** Regions excluded at 95% CL in the q^* coupling vs. mass plane.

in the coupling vs. mass plane. Comparing the CDF measurement with previously reported limits shown in Fig. 11b, we see that the simplest model of excited quarks is excluded for mass less than 540 GeV/c^2 at 95% CL.

7. Conclusions

Measurements of prompt photon production at the Fermilab Collider are precision tests of next-to-leading-order QCD and constrain the gluon distribution of the proton. Also, the diphoton candidate mass distribution and photon candidate + jet mass distribution are interesting probes of possible new physics beyond the standard model.

References

1. H. Baer, J. Ohnemus, and J. F. Owens *Phys. Lett.* **B234**(1990)127.
2. F. Abe *et al.* (CDF Collaboration), *Nucl. Instr. Meth.* **A271**(1988)387.
3. S. Abachi *et al.* (D0 Collaboration), *Nucl. Instr. Meth.* **A338** (1994)185.
4. F. Abe *et al.* (CDF Collaboration), *Phys. Rev. Lett.* **68**(1992)2734;
   F. Abe *et al.* (CDF Collaboration), *Phys. Rev.* **D48**(1993)2998.
5. J. Botts *et al.* (CTEQ Collaboration), *Physics Letters* **B304**(1993)159.
6. A. Martin, R. Roberts, and W. Stirling, *Physics Letters* **B309**(1993)492.
7. F. Abe *et al.*, *Phys. Rev. Lett.* **62**(1989)3020.
8. F. Abe *et al.*, *Phys. Rev. Lett.* **71**(1993)679.
9. B. Bailey, J. F. Owens and J. Ohnemus, *Phys. Rev.* **D46**(1992)2018.
10. F. Abe, *et al.* (CDF Collaboration), *Phys. Rev. Lett.* **70**(1993)2232.
11. U. Baur, I. Hinchliffe and D. Zeppenfeld, Int. Journal of Mod. Phys. **A2**(1987)1285;
    U. Baur, M. Spira, and P. Zerwas, Phys. Rev. **D42**(1990)815.
12. F. Abe *et al.* (CDF Collaboration), *Phys. Rev. Lett.* **72**(1994)3004.